Inorganic Chemistry

Article

pubs.acs.org/IC

Oxygenative Aromatic Ring Cleavage of 2-Aminophenol with Dioxygen Catalyzed by a Nonheme Iron Complex: Catalytic Functional Model of 2-Aminophenol Dioxygenases

Sayanti Chatterjee and Tapan Kanti Paine*

Department of Inorganic Chemistry, Indian Association for the Cultivation of Science, 2A & 2B Raja S. C. Mullick Road, Jadavpur, Kolkata 700032, India

Supporting Information

ABSTRACT: 2-Aminophenol dioxygenases catalyze the oxidative ring cleavage of 2-aminophenol to 2-picolinic acid using O_2 as the oxidant. Inspired by the reaction catalyzed by these nonheme iron enzymes, a biomimetic iron(III)-2-amidophenolate complex, $[(t\text{Bu-L}^{Me})\text{Fe}^{III}(4,6\text{-di-}t\text{Bu-AP})](ClO_4)$ (**1a**) of a facial tridentate ligand (tBu-L^{Me} = 1-[bis(6-methyl-pyridin-2-yl)-methyl]-3-*tert*-butyl-urea and 4,6-di-tBu-H$_2$AP = 2-amino-4,6-di-*tert*-butylphenol) bearing a urea group have been isolated. The complex reacts with O_2 to cleave the C−C bond of 4,6-di-tBu-AP regioselectively and catalytically to afford 4,6-di-*tert*-butyl-2-picolinic acid. An iron(II)-chloro complex $[(t\text{Bu-L}^{Me})\text{Fe}^{II}Cl_2(MeOH)]$ (**1**) of the same ligand also cleaves the aromatic ring of 4,6-di-tBu-AP catalytically in the reaction with O_2. To assess the effect of urea group on the ring cleavage reaction of 2-aminophenol, two iron complexes, $[(\text{BA-L}^{Me})_2\text{Fe}^{II}{}_2Cl_4]$ (**2**) and $[(\text{BA-L}^{Me})\text{Fe}^{III}(4,6\text{-di-}t\text{Bu-AP})](ClO_4)$ (**2a**), of a tridentate ligand devoid of urea group (BA-L^{Me} = benzyl-[bis(6-methyl-pyridin-2-yl)-methyl]-amine) have been isolated and characterized. Although the iron complexes (**1** and **1a**) of the ligand with urea group display catalytic reaction, the iron complexes (**2** and **2a**) of the ligand without urea group do not exhibit catalytic aromatic ring fission reactivity. The results support the role of urea group in directing the catalytic reactivity exhibited by **1** and **1a**.

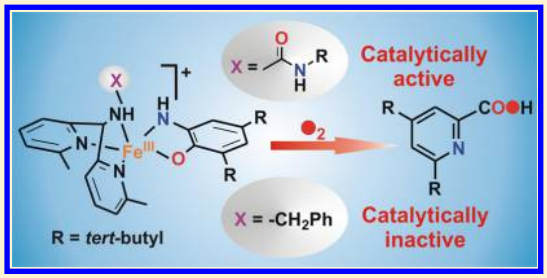

INTRODUCTION

Aromatic ring-cleaving dioxygeneases belong to the family of nonheme enzymes that are involved in the biodegradation of aromatic molecules with the incorporation of both atoms of dioxygen into cleavage products.[1−3] 2-Aminophenol-1,6 dioxygenase (APD) is a ring-cleaving enzyme and belongs to a small group of extradiol dioxygenases. APD, involved in the biodegradation of nitroaromatics in soil, was first isolated and purified from soil bacteria *Pseudomonas pseudoalcaligenes*.[4−8] The biodegradation process is initiated by partial reduction of nitrobenzene to hydroxylaminobenzene and further to 2-aminophenol.[7,9−11] The C−C bond cleavage of 2-aminophenol with molecular oxygen is then catalyzed by APD. The C−C cleavage product, 2-aminomuconic acid semialdehyde, spontaneously loses a water molecule to form 2-picolinic acid (Scheme 1).[8] A related enzyme, 3-hydroxyanthranilate-3,4-dioxygenase (HAD), isolated from *Saccharomyces cerevisiae*, catalyzes the ring opening of 3-hydroxyanthranilate to quinolinic acid in the tryptophan catabolism pathway (Scheme 1).[12−15] Very recently, the crystal structures of APD from *Comamonas* sp. strain CNB-1 in complex with the lactone intermediate (4*Z*,6*Z*)-3-iminooxepin-2(3H)-one and the product 2-aminomuconic acid-6-semialdehyde and in complex with the suicide inhibitor 4-nitrocatechol have been reported.[16] In the active site of APD, the iron center is ligated by His13, His62, and Glu251 in the first coordination sphere, whereas Tyr129 and His195 residues are present in the second coordination sphere. 2-Aminophenol substrate binds to the iron(II) center in a bidentate mode to initiate the aromatic ring cleavage reaction by activating dioxygen. Mutation studies on APD from *Comamonas* sp. with a mutant Y129F has been reported to exhibit complete loss of enzymatic activity toward 2-aminophenol.[16] On the basis of mutation studies, a hydrogen bonding interaction between the oxygen of 2-aminophenol and the OH group of Tyr129 has been proposed where the tyrosinate residue (Tyr 129) deprotonates the hydroxyl group of 2-aminophenol during the catalytic reaction.

Scheme 1. Reactions Catalyzed by APD and HAD

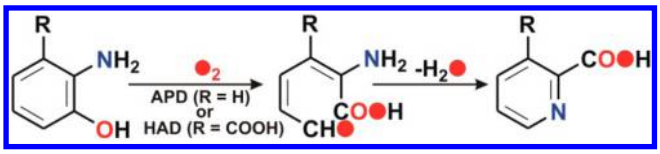

The oxidative transformation of 2-aminophenol to 2-picolinic acid by molecular oxygen has attracted the attention of biomimetic chemists to develop synthetic models of 2-aminophenol dioxygenases. Fiedler et al. have reported the synthesis and characterization of iron(II)-2-iminobenzo-semiquinonato radical complexes relevant to an intermediate

Received: November 7, 2014

DOI: 10.1021/ic502658p
Inorg. Chem. XXXX, XXX, XXX−XXX

proposed for APD.[17−19] Recently, we have reported the dioxygen reactivity of six-coordinate iron(II)-2-aminophenolate complexes of an N_4 ligand using substituted 2-aminophenols. The complexes have been shown to react with dioxygen under ambient conditions to afford substituted 2-picolinic acids mimicking the function of 2-aminophenol dioxygenases (APD and HAD).[20,21] These model complexes provide useful insight into the mechanism of aromatic ring cleavage of 2-aminophenols. However, all these model complexes exhibit stoichiometric reactivity and as of now there is no report on catalytic model of 2-aminophenol dioxygenases. In developing the catalytic model, one of the major challenges is to regulate the interactions between second sphere residues and substrate in synthetic catalysts as in the enzyme−substrate complex.[22,23] The importance of second coordination sphere has been shown in bioinorganic model chemistry.[16,24−30] The effect of second coordination sphere has also been documented on the dioxygen reactivity of biomimetic complexes and on the stability of metal−oxygen oxidants.[27,31−35]

With an objective to develop catalytic models of 2-aminophenol dioxygenases, we have explored the iron-aminophenolate chemistry of a facial tridentate ligand bearing urea group (Chart 1). The urea-bearing ligand is expected to provide

Chart 1. Ligands and Aminophenol Substrate

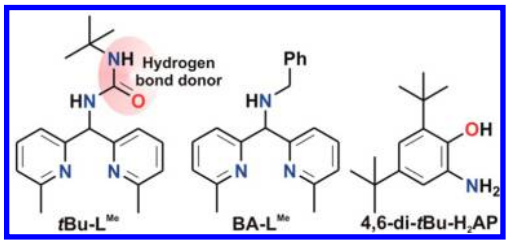

the necessary second coordination effect through hydrogen-bonding interactions. To probe the effect of urea group on the reactivity of iron-2-aminophenolate complex toward dioxygen, we have also studied the reactivity of two iron complexes supported by another facial N_3 ligand devoid of urea moiety. In this article, we report the synthesis and characterization of two iron(II)-chloro complexes, [(*t*Bu-L^{Me})$Fe^{II}Cl_2$(MeOH)] (**1**),[36] and [(BA-L^{Me})$_2Fe^{II}_2Cl_4$] (**2**), and two iron(III)-2-amidophenolate complexes, [(*t*Bu-L^{Me})Fe^{III}(4,6-di-*t*Bu-AP)](ClO_4) (**1a**) and [(BA-L^{Me})Fe^{III}(4,6-di-*t*Bu-AP)](ClO_4) (**2a**) (*t*Bu-L^{Me} = 1-[bis(6-methyl-pyridin-2-yl)-methyl]-3-*tert*-butyl-urea, BA-L^{Me} = benzyl-[bis(6-methyl-pyridin-2-yl)-methyl]-amine, 4,6-di-*t*Bu-H_2AP = 2-amino-4,6-di-*tert*-butylphenol) (Chart 1). The pH-dependent regiospecific C−C bond cleavage of 4,6-di-*t*Bu-H_2AP on the iron complexes and the role of urea group on the catalytic ring opening reactivity of 2-aminophenol are discussed.

RESULTS AND DISCUSSION

Synthesis and Characterization. The iron(II)-chloro complexes, **1** and **2**, were isolated by mixing $FeCl_2$ with *t*Bu-L^{Me} and BA-L^{Me}, respectively, in dichloromethane.[36] The iron(III)-2-amidophenolate complexes (**1a** and **2a**) were isolated from the reactions of a basic solution of 2-amino-4,6-di-*tert*-butylphenol with the respective iron(II)-chloro complex under controlled O_2 atmosphere. The iron(III)-amidophenolate complexes can also be isolated from the reaction of the respective ligand (*t*Bu-L^{Me} or BA-L^{Me}), iron(III) perchlorate hydrate and 4,6-di-*t*Bu-H_2AP in the presence of 2 equiv of triethylamine in methanol under inert atmosphere (see Experimental Section). The violet solution of complex **1a** in acetonitrile displays intense and broad absorption bands at 548 and 880 nm, whereas complex **2a** displays absorption bands at 618 and 1002 nm, typical of amidophenolate-to-iron(III) charge-transfer (CT) transitions (Figure S1, Supporting Information (SI)). The ^{1}H NMR spectra of **1**[36] and **2** display paramagnetically shifted resonances of the protons as observed with high-spin iron(II) complexes (Figure S2, SI). The room temperature magnetic moments of 5.98 μ_B for **1a** and 5.96 μ_B for **2a** are indicative of the high-spin nature of the iron(III) complexes. The X-band EPR spectra of both **1a** and **2a** at 77 K display rhombic signals typical of high-spin iron(III) complexes (Figure S3, SI).

The crystal structure of the mononuclear iron(II)-dichloro complex **1** has recently been reported by our group.[36] For solid-state structural verification, single crystals of **2** were isolated by diffusion of diethyl ether into a mixture of dichloromethane−methanol solution of the complex. X-ray crystal structure of the neutral complex (**2**) reveals a chloro-bridged di-iron complex where each six-coordinate iron center adopts distorted octahedral coordination geometry (Figure 1). The complex

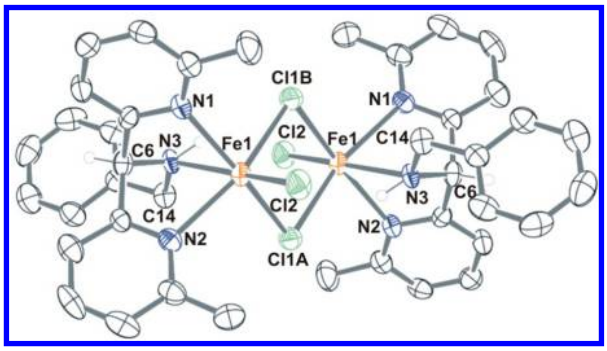

Figure 1. ORTEP plot of complex **2** with 40% thermal ellipsoid parameters. All hydrogen atoms except those on C6 and N3 have been omitted for clarity. Selected bond lengths [Å] and angles [°] for **2**: Fe(1)−N(1) 2.358(5), Fe(1)−N(2) 2.317(5), Fe(1)−N(3) 2.242(5), Fe(1)−Cl(1A) 2.4932(18), Fe(1)−Cl(1B) 2.5402(19), Fe(1)−Cl(2) 2.3109(19), C(6)−N(3) 1.462(7), C(14)−N(3) 1.474(7), N(2)−Fe(1)−N(3) 72.16(18), N(1)−Fe(1)−N(3) 72.51(19), N(1)−Fe(1)−N(2) 86.32(18), N(1)−Fe(1)−Cl(1A) 93.60(14), N(2)−Fe(1)−Cl(1A) 166.55(14), N(3)−Fe(1)−Cl(1A) 94.97(13), N(1)−Fe(1)−Cl(1B) 160.48(15), N(2)−Fe(1)−Cl(1B) 88.95(13), N(3)−Fe(1)−Cl(1B) 88.01(14), N(1)−Fe(1)−Cl(2) 98.91(15), N(2)−Fe(1)−Cl(2) 95.67(14), N(3)−Fe(1)−Cl(2) 165.21(13), Cl(1A)−Fe(1)−Cl(2) 97.63(7), Cl(1A)−Fe(1)−Cl(1B) 86.68(6), Cl(1B)−Fe(1)−Cl(2) 100.40(7).

consists of two identical monomeric [FeLCl] units held together through two bridging chloro ligands. One face of the octahedron at each iron center is coordinated by two pyridine nitrogens (N1 and N2) and an amine nitrogen atom (N3). The other face is occupied by three chloride ions where the Fe−Cl2 bond is shorter compared to the bridging Fe1−Cl bonds. One pyridine nitrogen (N1), the amine nitrogen (N3), and the two chloride atoms (Cl2 and Cl1B) occupy the equatorial plane. The pyridine nitrogen (N2) and the other bridging chloro atom (Cl1A) form the axial plane with the Cl1A−Fe1−N2 angle of 166.55 (14). The average iron−nitrogen distance (2.31 Å) is close to that observed in complex **1**.[36] Two metal ions along with the two bridging chloro atoms form a four-membered [Fe_2Cl_2] core with the Fe···Fe

DOI: 10.1021/ic502658p
Inorg. Chem. XXXX, XXX, XXX−XXX

separation of 3.661 Å. Although complex **2** is dimeric in the solid state, optical titration reveals that 1 equiv of **2** consumes 2 equiv of 4,6-di-*t*Bu-H_2AP to form 2 equiv of complex **2a** (Figure S4, SI). Complex **1**, being a mononuclear complex, consumes 1 equiv of 4,6-di-*t*Bu-H_2AP to quantitatively generate the monomeric iron(III)-amidophenolate complex **1a** (Figure S5, SI). Unfortunately, all attempts to isolate single crystals of the iron(III)-2-amidophenolate complexes **1a** and **2a** failed. The structures of **1a** and **2a** were therefore optimized by DFT calculations (Figure S6 and S7, SI). The ligand *t*Bu-L^{Me} has been reported to coordinate to the iron(II) center in [(*t*Bu-L^{Me})$Fe^{II}Cl_2$(MeOH)] through three nitrogen donors (NNN binding mode).[36] However, in iron(III)-amidophenolate complex **1a**, the ligand may exhibit several binding modes. The urea group of *t*Bu-L^{Me} can coordinate either via a nitrogen atom or through the oxygen atom. Therefore, the structure of **1a** was optimized considering NNN, NNO, monoanionic NNN, and monoanionic NNO binding modes of the ligand. The iron complex in S = 5/2 spin state with NNN binding mode of the ligand is found to be energetically more favorable than that with NNO binding mode (Tables S1 and S2, SI). The DFT calculations on **1a** with the monoanionic NNN form of the ligand, when performed using various functionals, did not converge to an energy minimized structure with S = 5/2 spin state. The energy for **1a** from DFT optimized structure with monoanionic NNN binding mode of the ligand (for S = 1/2 spin state) is energetically higher than the complex with neutral NNN binding mode (Table S3, SI). The structure of the complex with monoanionic NNO binding mode of the ligand, however, could not be optimized. From the optimized geometries (Figures S6 and S7, SI), it is observed that the dianionic 2-amidophenolate binds to the iron center in a bidentate mode in both the five-coordinate iron(III) complexes. With the NNN form of the ligand in **1a**, a moderate H-bonding interaction between the N−H of urea moiety and the nitrogen atom of the coordinated aminophenol is observed with the N···N distance of 3.1 Å and the N−H···N angle of 155.6° (Figure S6a, SI). However, no such interaction is observed with the NNO form of the ligand (Figure S6b, SI).

Reactivity of the Complexes toward Dioxygen. Both the iron(III)-2-amidophenolate complexes **1a** and **2a** are reactive toward dioxygen. For complex **1a**, during the reaction with O_2 the CT bands at 548 and 880 nm gradually diminish and the violet solution turns light green over a period of 3 h (Figure S8, SI). The ^{1}H NMR spectrum of the organic product obtained from the oxidized solution reveals 87% conversion of 2-amino-4,6-di-*tert*-butylphenol to a mixture of 4,6-di-*tert*-butyl-2*H*-pyran-2-one (20%) and 4,6-di-*tert*-butyl-2-picolinic acid (67%) (Scheme 2 and Figure S9, SI). For complex **2a**, the CT bands at 618 and 1002 nm slowly decay in less than 1 h (Figure S10, SI). Analyses of organic products by ^{1}H NMR spectroscopy indicate a quantitative transformation of 4,6-di-*t*Bu-H_2AP to 4,6-di-*tert*-butyl-2-picolinic acid (80%) and 4,6-di-*tert*-butyl-2*H*-pyran-2-one (20%) (Scheme 2).

Scheme 2. Reaction of Iron(III)-2-amidophenolate Complexes (1a and 2a) with O_2

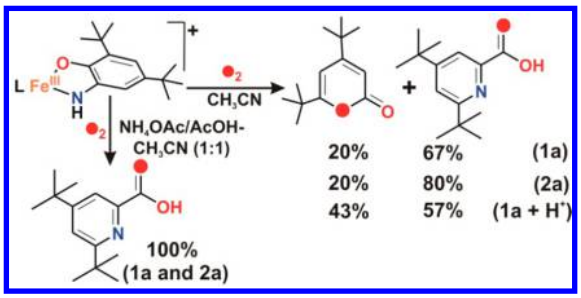

Recently, we reported an iron(III)-catecholate complex supported by *t*Bu-L^{Me} ligand where the extent of C−C bond cleavage of catechol has been shown to enhance dramatically in the presence of a protic acid.[36] The reaction of **1a** with O_2 in the presence of 1 equiv of pyridinium perchlorate exhibits a quantitative transformation of 4,6-di-*t*Bu-H_2AP to a mixture of 4,6-di-*tert*-butyl-2*H*-pyran-2-one (43%) and 4,6-di-*tert*-butyl-2-picolinic acid (57%) (Scheme 2, Figure S11, SI). At low concentration of pyridinium perchlorate, the reaction is not quantitative. On the other hand, the presence of excess pyridinium perchlorate (more than 1 equiv) lowers the yield of the C−C bond cleavage products probably due to the decomposition of the metal complex. Quantitative C−C bond cleavage is observed only with 0.8−1.0 equiv of pyridinium perchlorate. The amount of pyridinium perchlorate not only controls the overall yield of the aminophenol cleavage products but also affects the distribution of products (Table S4 and Figure S12, SI). The GC-mass spectrum of organic products (2-picolinic acid was esterified with diazomethane) shows two distinct ion peaks at m/z = 208 and 249 with the expected fragmentation patterns of 4,6-di-*tert*-butyl-2*H*-pyran-2-one and methyl-4,6-di-*tert*-butyl-2-picolinate (Figure 2a,b). When the reaction is carried out with $^{18}O_2$, the ion peak at m/z = 208 is shifted two mass unit higher to m/z = 210 and the peak at m/z = 249 is shifted to m/z = 251 (Figure 2c,d). Partial loss of the labeled oxygen in methyl-4,6-di-*tert*-butyl-2-picolinate occurred due to elimination of a water molecule during esterification of the acid. The labeling experiment confirms the incorporation of one ^{18}O atom into each of the cleavage products. Of note, complexes **1** and **2** react with 4,6-di-*t*Bu-H_2AP in the presence of dioxygen to afford almost same amounts of C−C bond cleavage products as observed with **1a** and **2a**, respectively. The iron(III)-2-amidophenolate complexes (**1a** and **2a**) are therefore functional models of 2-aminophenol dioxygenases.

Interestingly, complex **1a** reacts with dioxygen at room temperature in a mixture of acetonitrile and ammonium acetate/acetic acid buffer (1:1; pH = 5.5) at a much faster rate (k_{obs} = 4.53 × 10^{-2} s^{-1}) (Figure 3). In the reaction, quantitative yield of 4,6-di-*tert*-butyl-2-picolinic acid is observed (Figure S13, SI). Although the buffer has no effect on the rate of the reaction of **2a** with dioxygen, the complex undergoes oxidative C−C bond cleavage to afford 4,6-di-*tert*-butyl-2-picolinic acid as the only product (Scheme 2).

Catalytic Reactivity. The catalytic aromatic ring fission reactivity of **1a** was studied in a mixture of acetonitrile and buffer at different pH. The use of buffer for catalytic experiments was initiated in order to develop a suitable experimental method for catalysis, where both deprotonation of aminophenol as well as proton supply necessary for C−C bond cleavage reaction would be available. In biological systems, pH plays a crucial role in controlling various biologically relevant oxidative transformation reactions.[37] Similar to that observed with a related iron(III)-catecholate complex of *t*Bu-L^{Me},[36] the catalytic activities of iron complexes **1** and **1a** not only depend on the concentration of substrate but also are affected by pH of the reaction medium. The use of buffer with higher or lower pH exhibits lower catalytic turnover number (TON). When the reaction is carried out in pure acetonitrile, the complexes (**1** or

DOI: 10.1021/ic502658p
Inorg. Chem. XXXX, XXX, XXX−XXX

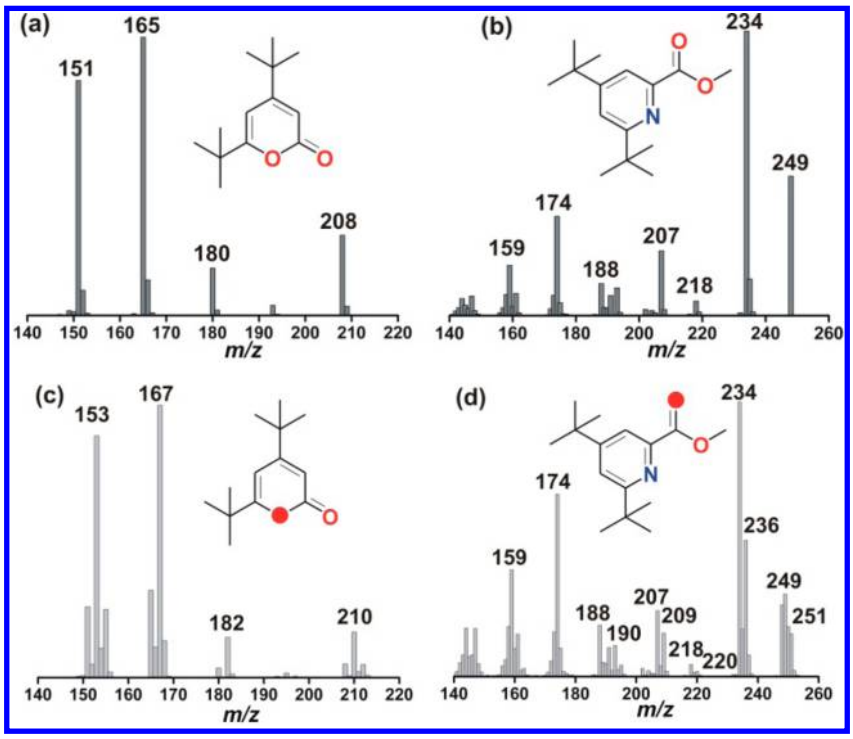

Figure 2. GC-mass spectra of organic products from **1a** after the reaction with $^{16}O_2$ (a and b) and $^{18}O_2$ (c and d). The metal ion was removed, and picolinic acid was esterified prior to analysis.

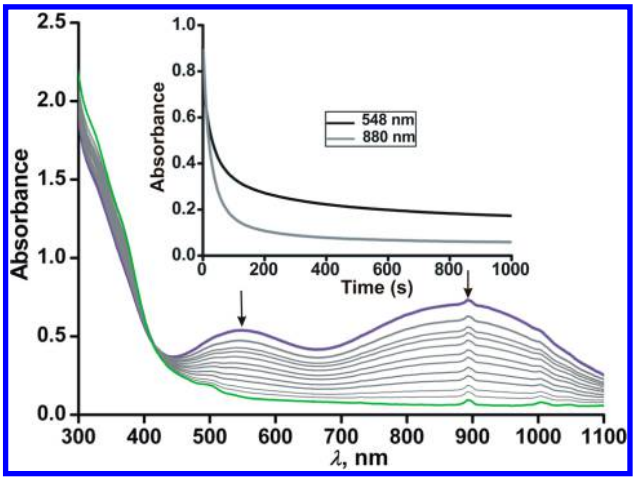

Figure 3. Optical spectral changes with time during the reaction of **1a** (0.5 mM solution in acetonitrile and NH_4OAc/AcOH buffer mixture (1:1) of pH = 5.5) with dioxygen at 298 K. Inset: plot of absorbance vs time.

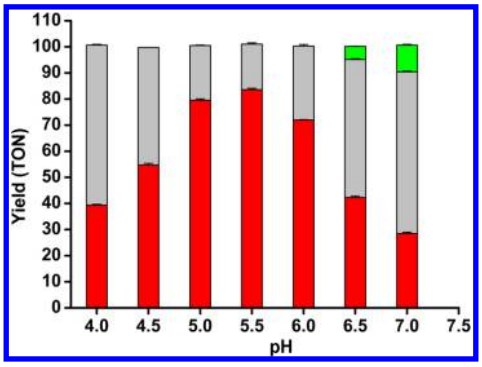

Figure 4. Plot of turnover number of products derived from 4,6-di-*t*Bu-H_2AP vs pH for complex **1a**.

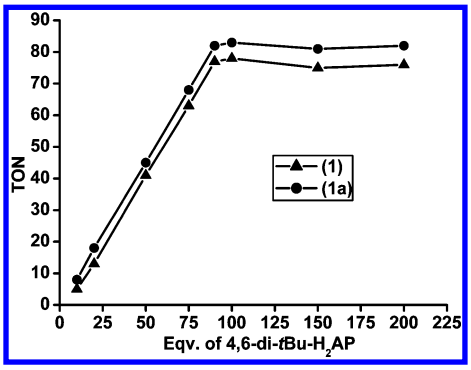

Figure 5. Plot of TON vs equiv of 4,6-di-*t*Bu-H_2AP added in the catalytic reaction with **1** and **1a**.

1a) do not exhibit catalytic turnover (for 4,6-di-*tert*-butyl-2-picolinic acid); the auto-oxidation product 3,5-di-*tert*-butylbenzoquinone is found as the major product. The auto-oxidation pathway gets inhibited in buffer medium, and an optimum pH of 5.5 is required for the highest catalytic efficiency (Figure 4). Similar results are obtained when the catalytic experiments are carried out in phthalate buffer.

With an increase in the amount of aminophenol (4,6-di-*t*Bu-H_2AP), the turnover number (TON) of 4,6-di-*tert*-butyl-2-picolinic acid increases (Figure 5). Complex **1a** is found to be an efficient catalyst with a maximum TON of 83 at pH = 5.5 after 5 h with 100 equiv of aminophenol (Figures 5 and S14, SI). When complex **1** is used as a catalyst under the same experimental conditions, a maximum TON of 82 is observed. The catalytic results with complex **1** support in situ formation of **1a** quantitatively in the reaction with aminophenol. On the contrary, complex **2a**, which shows comparable reactivity to **1a** under stoichiometric conditions, does not exhibit catalytic

DOI: 10.1021/ic502658p
Inorg. Chem. XXXX, XXX, XXX−XXX

Scheme 3. Proposed Catalytic Pathway for the Regiospecific Aromatic Ring Cleavage of 2-Aminophenol Using O_2 as the Oxidant

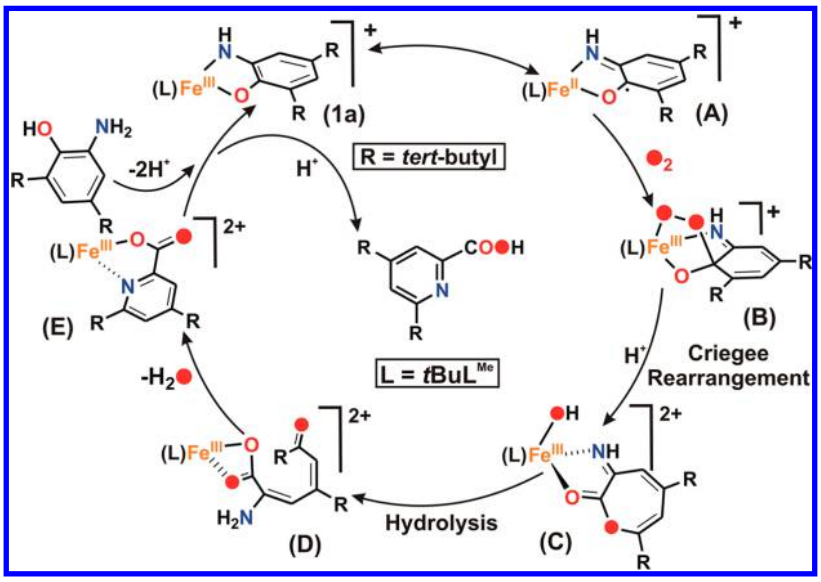

reactivity under similar experimental conditions and at various pH. The iron complexes of *t*Bu-L^{Me} ligand represent the first catalytic models of 2-aminophenol dioxygenases.

The reaction mechanism proposed for the catalytic cycle of both APD and HAD involves iron(II) in the active site.[15,16,38] The ring fission reactivity exhibited by the iron(II) complex (**1**) and by the iron(III)-2-amidophenolate complex (**1a**) strongly indicates that the catalytic reaction proceeds, unlike the enzymes, through an iron(III)-amidophenolate complex. Amidophenolate, being a redox noninnocent ligand, transfers one electron to the iron(III) center of **1a** with the generation of an iron(II)-2-iminobenzosemiquinone radical species (**A**). As reported for other model iron-aminophenolate complexes,[20,21] intermediate species **A** (Scheme 3) is proposed to react with dioxygen to generate an iron(III)-alkylperoxo intermediate (**B**). The urea group on the ligand is expected to interact with the peroxo species favoring a proton-assisted Criegee-type rearrangement via alkenyl migration to form **C**. The lactone ring in **C** gets hydrolyzed to afford the regiospecific C−C bond cleavage product, 4,6-di-*tert*-butyl-2-picolinic acid. In the presence of excess aminophenol substrate, complex **1a** is regenerated to get into the catalytic cycle.

In the catalytic cycle, it is likely that the resting state of the reaction after the first cycle gets destabilized in case of **1**. To test the hypothesis if picolonic acid product inhibits the reaction of **2** and not that of **1**, we have isolated iron(III)-2-picolinate complexes, $[(t\text{Bu-L}^{Me})\text{Fe}^{III}(\text{picolinate})]^{2+}$ (**1b**) and $[(\text{BA-L}^{Me})\text{Fe}^{III}(\text{picolinate})]^{2+}$ (**2b**) (see Experimental Section). Reaction of **1b** with 1 equiv of 4,6-di-*t*Bu-H_2AP in a mixture of acetonitrile and acetate buffer regenerates **1a** immediately, which is evident from the characteristic LMCT bands at 548 and 880 nm (Figure 6). Thus, the picolinate group in the iron(III)-picolinate complex of the urea ligand is more labile for incoming substrate 4,6-di-*t*Bu-H_2AP, and the product-bound form (see **E** in Scheme 3) of the catalyst is destabilized favoring catalyst regeneration for **1a**. On the contrary, the iron(III)-picolinate complex (**2b**) of BA-L^{Me} does not regenerate the iron(III)-amidophenolate complex even after treatment with an excess amount of 4,6-di-*t*Bu-H_2AP (Figure S15, SI). The

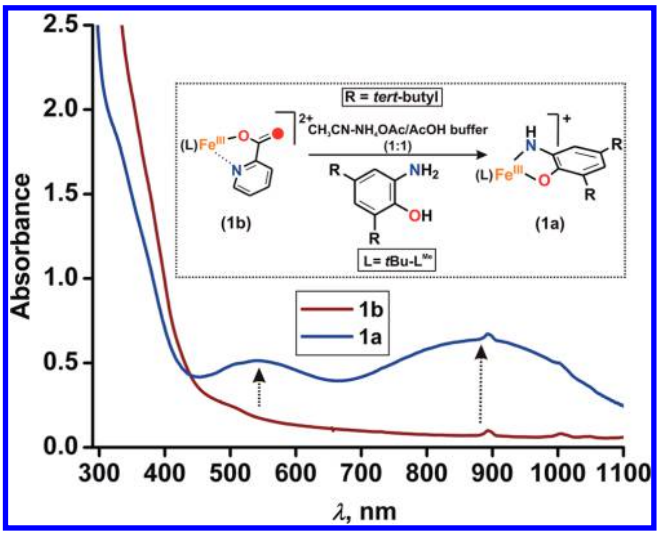

Figure 6. Optical spectral change upon addition of 4,6-di-*t*Bu-H_2AP to an acetonitrile-acetate buffer solution (0.5 mM) of iron(III)-picolinate complex, **1b**.

formation of a stable product-bound complex as the resting state prevents the catalytic reactivity in **2**.

The iron(III)-2-amidophenolate complexes (**1a** and **2a**) have similar primary coordination sphere around the iron center, but the only difference is that the urea group in **1a** (*t*Bu-L^{Me}) can provide necessary second sphere interaction via hydrogen bonding interaction; however, the ligand (BA-L^{Me}) in **2a** cannot engender such interaction. DFT optimized geometry of the peroxo intermediate (**B**) reveals a hydrogen bonding interaction between a nitrogen of urea group and a peroxo oxygen with the N···O distance of 2.79 Å and the N−H···O angle of 139.1° (Table S5 and Figure S16, SI). In the reaction pathway, the urea group may also supply the proton to the peroxo intermediate leading to the cleavage of the O−O bond. The deprotonated urea moiety then can pick up a proton at a later stage in the catalytic cycle. The effect of proton (buffer) on the rate of reaction and on the catalytic activity of **1a** indicates the involvement of the urea group in the second

DOI: 10.1021/ic502658p
Inorg. Chem. XXXX, XXX, XXX−XXX

coordination sphere. However, in the absence of crystal structure of complex **1a** or **E**, the exact mode of interaction between the urea group and the substrate/product cannot be unambiguously predicted.

■ CONCLUSION

In conclusion, we have isolated and characterized two iron(II)-chloro complexes and two iron(III)-2-amidophenolate complexes of facial tridentate ligands. All the iron complexes are found to exhibit regiospecific cleavage of the C−C bond adjacent to the phenolic OH group of 2-amino-4,6-di-*tert*-butylphenol to form 4,6-di-*tert*-butyl-2-picolinic acid. The iron complexes of the ligand containing a urea group exhibit catalytic aromatic ring cleavage of 2-aminophenol in acetonitrile-acetate buffer mixture (1:1) at pH = 5.5. On the other hand, the iron complexes of the ligand without a urea group studied in this work do not show catalytic aromatic ring cleavage reactivity. The results reported here support the role of urea group on catalytic turnovers. The strategy of using a ligand with hydrogen bond donor group has been successfully employed in developing a nonheme iron catalyst for the conversion of 2-aminophenol to 2-picolinic acid using O_2 as the oxidant. Detailed structural and mechanistic studies are being pursued to unravel the role of urea group in the catalytic pathway.

■ EXPERIMENTAL SECTION

All chemicals and reagents were obtained from commercial sources and were used without further purification unless otherwise noted. Solvents were distilled and dried before use. Preparation and handling of air-sensitive materials were carried out under an inert atmosphere in a glovebox. The ligand *t*Bu-L^{Me} and the complex [(*t*Bu-L^{Me})-Fe^{II}Cl$_2$(MeOH)] (**1**) were prepared according to a procedure reported in the literature.[36]

Fourier transform infrared spectroscopy on KBr pellets was performed on a Shimadzu FT-IR 8400S instrument. Elemental analyses were performed on a PerkinElmer 2400 series II CHN analyzer. Electro-spray ionization (ESI) mass spectra were recorded with a Waters QTOF Micro YA263 instrument. Solution electronic spectra (single and time-dependent) were measured on an Agilent 8453 diode array spectrophotometer. All room temperature NMR spectra were collected on a Bruker Avance 500 MHz spectrometer. Room temperature magnetic data were collected on Gouy balance (Sherwood Scientific, Cambridge, U.K.). Diamagnetic contributions were calculated for each compound using Pascal's constants. X-band EPR measurements were performed on a JEOL JES-FA 200 instrument. GC-MS measurements were carried out with a PerkinElmer Clarus 600 using Elite 5 MS (30 m × 0.25 mm × 0.25 μm) column with a maximum temperature 300 °C. Labeling experiments were carried out with $^{18}O_2$ gas (99 atom %) or H_2O^{18} (98 atom %) purchased from Icon Services Inc., U.S.A.

Synthesis. *Ligand BA-L^{Me}.* To a solution of bis(6-methylpyridin-2-yl)methanamine (0.84 g, 4 mmol) in dry methanol (10 mL) was added benzaldehyde (408 μL, 4 mmol) and stirred for 24 h. To the resulting solution, sodium cyanoborohydride (0.28 g, 4.5 mmol) was added and stirred overnight. The yellow solution thus formed was treated with concentrated hydrochloric acid until the effervescence ceased. The solvent was then removed and the residue was treated with a saturated solution of sodium bicarbonate. The organic product was extracted with dichloromethane. The organic layer was then dried over anhydrous sodium sulfate, and the solvent was removed to isolate a pale yellow oil. Yield: 0.90 g (75%). ^{1}H NMR (CDCl$_3$, 500 MHz): δ (ppm) 7.52 (t, 2H, J = 7.8 Hz), 7.37 (d, 2H, J = 7 Hz), 7.33 (t, 2H, J = 7.5 Hz), 7.22 (d, 1H, J = 7 Hz), 7.19 (d, 2H, J = 8 Hz), 7.01 4(d, 2H, J = 7 Hz), 5.13 (s, 1H), 3.83 (s, 2H) 2.55 (s, 6H). ESI-MS (positive ion mode, acetonitrile): m/z = 326.21 (10%. [M + Na]$^+$, 304.20 (100%, [M + H]$^+$).

*[(tBu-L^{Me})Fe^{III}(4,6-di-tBu-AP)](ClO$_4$) (**1a**).* To a solution of *t*Bu-L^{Me} ligand (0.16 g, 0.5 mmol) in methanol was added Fe(ClO$_4$)$_3$·6H$_2$O (0.23 g, 0.5 mmol). To the resulting yellow solution was added a methanolic solution (5 mL) of 2-amino-4,6-di-*tert*-butylphenol (0.11 g, 0.5 mmol) and triethylamine (130 μL). The resulting dark violet solution was stirred at room temperature under nitrogen atmosphere for 2 h. A violet precipitate was formed, which was filtered and washed with diethyl ether to isolate a violet crystalline solid. Yield: 0.25 g (73%). Elemental Anal. Calcd (%) for $C_{32}H_{45}ClFeN_5O_6$ (687.03 g/mol): C, 55.94; H, 6.60; N, 10.19. Found: C, 55.86; H, 6.43; N, 10.17. IR (KBr): 3367(br), 3093, 3068, 2958(vs), 2908, 2867, 1641, 1593, 1552(vs), 1456(vs), 1417, 1390, 1361, 1234, 1176, 1145, 1105(s), 1043, 999, 902, 831, 804, 765, 748, 659, 628 cm^{-1}. UV−vis in MeCN: λ, nm (ε, M^{-1}cm^{-1}): 548 (1100), 880 (1400). Magnetic moment (298 K): 5.98 μ_B.

*[(BA-L^{Me})$_2$Fe$^{II}_2$Cl$_4$] (**2**).* To a solution of BA-L^{Me} ligand (0.15 g, 0.5 mmol) in dichloromethane was added FeCl$_2$ (0.064 g, 0.5 mmol). The resulting yellow solution was stirred for 1 h to precipitate a yellow solid. The precipitate was filtered and then washed with dichloromethane to isolate a yellow powder. X-ray quality yellow single crystals were isolated by diffusion of diethyl ether into a mixture of dichloromethane-methanol solution of the complex. Yield: 0.38 g (88%). Elemental Anal. Calcd (%) for $C_{40}H_{42}Cl_4Fe_2N_6$ (860.30 g/mol): C, 55.84; H, 4.92; N, 9.77. Found: C, 55.74; H, 4.83; N, 9.94. IR (KBr): 3396(br), 3060, 2923, 2088, 1639, 1604(s), 1571(m), 1460(vs), 1380, 1159, 765, 703 cm^{-1}. Magnetic moment (298 K): 6.90 μ_B.

*[(BA-L^{Me})Fe^{III}(4,6-di-tBu-AP)](ClO$_4$) (**2a**).* To a solution of BA-L^{Me} (0.15 g, 0.5 mmol) in methanol was added Fe(ClO$_4$)$_3$·6H$_2$O (0.22 g, 0.5 mmol). The resulting yellow solution was then treated with a methanolic solution (5 mL) of 2-amino-4,6-di-*tert*-butylphenol (0.11 g, 0.5 mmol) and triethylamine (130 μL). The resulting dark violet solution was stirred at room temperature under nitrogen atmosphere for 2 h. The solvent was removed under vacuum, and the residue was washed with dichloromethane. The filtrate was concentrated and kept for layer diffusion with hexane to isolate a crystalline violet complex. Yield: 0.24 g (70%). Elemental Anal. Calcd (%) for $C_{34}H_{42}ClFeN_4O_5$ (678.02 g/mol): C, 60.23; H, 6.24; N, 8.26. Found: C, 60.38; H, 6.02; N, 8.12. IR (KBr): 3450(br), 3236, 3137, 2929, 1604(s), 1569(m), 1461(s), 1382, 1244, 1143, 1115, 1090 (vs), 1031, 1006, 757, 630 cm^{-1}. UV−vis in MeCN: λ, nm (ε, M^{-1}cm^{-1}): 618 (1040), 1002 (780). Magnetic moment (298 K): 5.96 μ_B.

*[(tBu-L^{Me})Fe^{III}(picolinate)](Cl$_2$) (**1b**).* To a solution of *t*Bu-L^{Me} ligand (0.16 g, 0.5 mmol) in methanol was added FeCl$_3$ (0.08 g, 0.5 mmol). To the resulting yellow solution was added a methanolic solution (5 mL) of sodium picolinate (0.07 g, 0.5 mmol). The solution slowly turned orange, and the solution was then stirred at room temperature under nitrogen atmosphere for 2 h. The solvent was removed under vacuum and the residue was washed with dichloromethane and filtered. The filtrate was concentrated and treated with diethyl ether to isolate an orange crystalline compound, **1b**·CH$_3$OH. Yield: 0.24 g (82%). Elemental Anal. Calcd (%) for $C_{25}H_{32}Cl_2FeN_5O_4$ (593.3 g/mol): C, 50.61; H, 5.44; N, 11.80. Found: C, 50.36; H, 5.17; N, 11.59. IR (KBr): 3360(br), 2974(s), 2972, 2898, 1645(vs), 1595, 1568, 1552, 1454, 1392, 1365, 1269, 1215, 1170, 1089, 1047(vs), 831, 879, 763, 703, 405, 383 cm^{-1}. Magnetic moment (298 K): 5.97 μ_B.

*[(BA-L^{Me})Fe^{III}(picolinate)](Cl$_2$) (**2b**).* To a solution of BA-L^{Me} (0.15 g, 0.5 mmol) in methanol was added FeCl$_3$ (0.08 g, 0.5 mmol). The yellow solution was then treated with a methanolic solution (5 mL) of sodium picolinate (0.07 g, 0.5 mmol). The resulting orange solution was stirred at room temperature under nitrogen atmosphere for 2 h. The solvent was removed in vacuum, and the residue was washed with dichloromethane and filtered. The filtrate was concentrated and treated with diethyl ether to isolate an orange solid, **2b**·CH$_3$OH. Yield: 0.22 g (81%). Elemental Anal. Calcd (%) for $C_{27}H_{29}Cl_2FeN_4O_3$ (584.3 g/mol): C, 55.50; H, 5.00; N, 9.59. Found: C, 54.90; H, 4.84; N, 9.69. IR (KBr): 3406(br), 3286, 3256, 3064, 3033, 2923, 2854,1627(vs), 1593(vs), 1568(s), 1460(s), 1377, 1290, 1261, 1240, 1161, 1093 1031,

DOI: 10.1021/ic502658p
Inorg. Chem. XXXX, XXX, XXX−XXX

1070, 1047, 1014, 912, 852, 825, 798, 761, 702, 640, 622, 441 cm^{-1}. Magnetic moment (298 K): 5.95 μ_B.

Analysis of Organic Products after Reaction with Oxygen. In a typical stoichiometric reaction, dry oxygen gas was bubbled through an acetonitrile solution (5 mL) of the iron(III)-2-amidophenolate complex (**1a** or **2a**) (0.020 mmol) for 2 min. For iron(II) complex (**1** or **2**), a similar procedure was followed in the presence of 1 equiv of 2-amino-4,6-di-*tert*-butylphenol and 2 equiv of triethylamine to generate the corresponding iron(III)-2-amidophenolate complexes. For catalytic experiments, acetonitrile and ammonium acetate/acetic acid buffer solution (2.5 mL of acetonitrile and 2.5 mL of acetic acid-acetate buffer, the concentration of the original buffer solution is 1.18 M) was used for all the complexes (0.02 mmol) in the presence of excess 2-amino-4,6-di-*tert*-butylphenol. The solution was allowed to stir at room temperature under oxygen environment. During the reaction, the violet solution turned deep green and finally to yellow. After the reaction, the solvent was removed under vacuum and the residue was treated with 10 mL of 3 M hydrochloric acid solution. The organic products were extracted with diethyl ether (3 × 15 mL), and the organic layer was dried over anhydrous sodium sulfate. After removal of solvent, the colorless residue was analyzed by GC-MS and ^{1}H NMR spectroscopy. ^{1}H NMR data for 2-amino-4,6-di-*tert*-butylphenol cleavage products (500 MHz, $CDCl_3$, 298 K): (i) 4,6-di-*tert*-butyl-2H-pyran-2-one (A): δ (ppm) 1.22 (s, 9H), 1.36 (s, 9H), 6.05 (m, 2H), (ii) 4,6-di-*tert*-butyl-2-picolinic acid (B): δ (ppm) 1.27 (s, 9H), 1.40 (s, 9H), 7.59 (s, 1H), 8.06 (s, 1H).

Methyl-4,6-di-tert-butyl-2-picolinate. The organic product, isolated from the reaction solution according to the procedure mentioned above, was reacted with excess diazomethane in dry diethyl ether (5 mL) at 0 °C. The reaction solution was stirred for 5 min. After removing the insoluble part, the clear ether layer was analyzed by GC-MS. ^{1}H NMR (500 MHz, $CDCl_3$, 298 K): δ (ppm) 7.92 (s, 1H), 7.49 (s, 1H), 3.97 (s, 3H), 1.26 (s, 9H), 1.40 (s, 9H).

X-ray Crystallographic Data Collection and Refinement and Solution of the Structure of 2. X-ray single-crystal data for **2** were collected at 120 K using Mo Kα (λ = 0.7107 Å) radiation on a SMART-APEX diffractometer equipped with CCD area detector. Data collection, data reduction, structure solution, and refinement were carried out using the software package of APEX II.[39] The structure was solved by direct method and subsequent Fourier analyses and refined by the full-matrix least-squares method based on F^2 with all observed reflections.[40] The non-hydrogen atoms were treated anisotropically.

Crystal data of **2**: MF = $C_{40}H_{42}Cl_4Fe_2N_6$, MW = 860.30, monoclinic, space group $C2/c$, a = 24.995(3), b = 13.8687(17), c = 16.1645(19) Å, α = 90.00°, β = 129.524(3)°, γ = 90.00°, V = 4322.3(9) Å^3, Z = 4, ρ = 1.322 mgm^{-3}, μMo Kα = 0.953 mm^{-1}, F(000) = 1776, GOF = 1.064. A total of 16 518 reflections were collected in the range $1.81 \leq \theta \leq 25.10$, 2202 of which were unique (R_{int} = 0.0857. $R1(wR2)$ = 0.0503 0.1440 for 237 parameters and 1719 reflections (I > 2σ(I)). CCDC 998584 contains the supplementary crystallographic data for this paper. The data can be obtained free of charge from the Cambridge Crystallographic Data Centre via www.ccdc.cam.ac.uk/data_request/cif.

Computational Calculation Details. Density functional theory (DFT) calculations of the complexes were performed using the Gaussian 09 program package.[41] Geometry of $[(L)Fe^{III}(AP)]^+$ (i.e., **1a** and **2a**) were optimized with the geometry obtained from the crystal structure of **1** and **2**, respectively. The geometry of the iron(III)-alkylperoxo intermediate from **1a** after reaction with dioxygen was also optimized. The calculations were performed using spin unrestricted formalism using WB97XD functional[42−44] with 6-31G(d) basis functions for N, C, H, O and effective core potential LANL2 along with LANL2DZ basis set on Fe atom.[45,46] The optimization of the complexes were also checked with B3LYP functional[43,44] with 6-311G basis set and TZVP basis set provided for all the atoms. The bond parameters and energetics obtained from optimizations using all three functional were found to be very similar. Geometry of $[(L)Fe^{III}(AP)]^+$ (**1a**) with all possible spin states and binding modes of the ligand were calculated. The iron(III)-amidophenolate complex with the NNN binding mode of the ligand and S = 5/2 spin state was found to be of lowest energy. Although the complex with monoanionic NNN binding mode was optimized only in S = 1/2 spin state, the complex with monoanionic NNO binding mode of the ligand could not be optimized in any spin state. The vibrational frequency calculations with the optimized geometries were performed to ensure the local minima with positive eigen values. The energies reported herein for the optimized geometries included zero-point and free-energy corrections.

■ ASSOCIATED CONTENT

Supporting Information

Crystallographic data in CIF format, spectral data, and Cartesian coordinates, energies and bond parameters for the DFT optimized structures. This material is available free of charge via the Internet at http://pubs.acs.org.

■ AUTHOR INFORMATION

Corresponding Author

*E-mail: ictkp@iacs.res.in. Fax: +91-33-2473-2805. Phone: +91-22-2473-4971.

Notes

The authors declare no competing financial interest.

■ ACKNOWLEDGMENTS

T.K.P. acknowledges the DST, Govt. of India (Project: SR/S1/IC-51/2010) and INSA (Project for Young Scientist Awardee) for financial support. Authors thank Dr. Ankan Paul and Mr. Sourav Bhunya of IACS for their help with DFT calculations. S.C. thanks CSIR, India, for a research fellowship. X-ray diffraction data were collected at the DST-funded National Single Crystal Diffractometer facility at the Department of Inorganic Chemistry, Indian Association for the Cultivation of Science.

■ REFERENCES

(1) Bugg, T. D. H.; Winfield, C. J. *Nat. Prod. Rep.* **1998**, *15*, 513−530.
(2) Fetzner, S. *Appl. Environ. Microbiol.* **2012**, *78*, 2505−2514.
(3) Vaillancourt, F. H.; Bolin, J. T.; Eltis, L. D. *Crit. Rev. Biochem. Mol. Biol.* **2006**, *41*, 241−267.
(4) Lendenmann, U.; Spain, J. C. *J. Bacteriol.* **1996**, *178*, 6227−6232.
(5) Wu, J.-F.; Sun, C.-W.; Jiang, C.-Y.; Liu, Z.-P.; Liu, S.-J. *Arch. Microbiol.* **2005**, *183*, 1−8.
(6) Takenaka, S.; Murakami, S.; Shinke, R.; Hatakeyama, K.; Yukawa, H.; Aoki, K. *J. Biol. Chem.* **1997**, *272*, 14727−14732.
(7) Somerville, C. C.; Nishino, S. F.; Spain, J. C. *J. Bacteriol.* **1995**, *177*, 3837−3842.
(8) He, Z.; Spain, J. C. *J. Ind. Microbiol. Biotechnol.* **2000**, *25*, 25−28.
(9) Nishino, S. F.; Spain, J. C. *Appl. Environ. Microbiol.* **1993**, *59*, 2520−2525.
(10) Wu, J.-f.; Jiang, C.-y.; Wang, B.-j.; Ma, Y.-f.; Liu, Z.-p.; Liu, S.-j. *Appl. Environ. Microbiol.* **2006**, *72*, 1759−1765.
(11) Ju, K.-S.; Parales, R. E. *Microbiol. Mol. Biol. Rev.* **2010**, *74*, 250−272.
(12) Li, X.; Guo, M.; Fan, J.; Tang, W.; Wang, D.; Ge, H.; Rong, H.; Teng, M.; Niu, L.; Liu, Q.; Hao, Q. *Protein Sci.* **2006**, *15*, 761−773.
(13) Zhang, Y.; Colabroy, K. L.; Begley, T. P.; Ealick, S. E. *Biochemistry* **2005**, *44*, 7632−7643.
(14) Colabroy, K. L.; Begley, T. P. *J. Bacteriol.* **2005**, *187*, 7866−7869.
(15) Dilović, I.; Gliubich, F.; Malpeli, G.; Zanotti, G.; Matković-Calogović, D. *Biopolymers* **2009**, *91*, 1189−1195.
(16) Li, D.-F.; Zhang, J.-Y.; Hou, Y.-J.; Liu, L.; Hu, Y.; Liu, S.-J.; Wang, D.-C.; Liu, W. *Acta Crystallogr.* **2013**, *D69*, 32−43.
(17) Bittner, M. M.; Lindeman, S. V.; Fiedler, A. T. *J. Am. Chem. Soc.* **2012**, *134*, 5460−5463.

DOI: 10.1021/ic502658p
Inorg. Chem. XXXX, XXX, XXX−XXX

(18) Bittner, M. M.; Kraus, D.; Lindeman, S. V.; Popescu, C. V.; Fiedler, A. T. *Chem.—Eur. J.* **2013**, *19*, 9686−9698.
(19) Bittner, M. M.; Lindeman, S. V.; Popescu, C. V.; Fiedler, A. T. *Inorg. Chem.* **2014**, *53*, 4047−4061.
(20) Chakraborty, B.; Paine, T. K. *Angew. Chem., Int. Ed.* **2013**, *52*, 920−924.
(21) Chakraborty, B.; Bhunya, S.; Paul, A.; Paine, T. K. *Inorg. Chem.* **2014**, *53*, 4899−4912.
(22) Zhao, M.; Wang, H.-B.; Ji, L.-N.; Mao, Z.-W. *Chem. Soc. Rev.* **2013**, *42*, 8360−8375.
(23) Rosati, F.; Roelfes, G. *ChemCatChem* **2010**, *2*, 916−927.
(24) Light, K. M.; Hangasky, J. A.; Knapp, M. J.; Solomon, E. I. *Dalton Trans.* **2014**, *43*, 1505−1508.
(25) Kovaleva, E. G.; Lipscomb, J. D. *Science* **2007**, *316*, 453−457.
(26) Saban, E.; Chen, Y.-H.; Hangasky, J. A.; Taabazuing, C. Y.; Holmes, B. E.; Knapp, M. J. *Biochemistry* **2011**, *50*, 4733−4740.
(27) Shook, R. L.; Borovik, A. S. *Inorg. Chem.* **2010**, *49*, 3646−3660.
(28) Feng, G.; Mareque-Rivas, J. C.; Martıín de Rosales, R. T.; Williams, N. H. *J. Am. Chem. Soc.* **2005**, *127*, 13470−13471.
(29) Linjalahti, H.; Feng, G.; Mareque-Rivas, J. C.; Mikkola, S.; Williams, N. H. *J. Am. Chem. Soc.* **2008**, *130*, 4232−4233.
(30) Comba, P.; Gahan, L. R.; Mereacre, V.; Hanson, G. R.; Powell, A. K.; Schenk, G.; Zajaczkowski-Fischer, M. *Inorg. Chem.* **2012**, *51*, 12195−12209.
(31) Lucas, R. L.; Zart, M. K.; Mukherjee, J.; Sorrell, T. N.; Powell, D. R.; Borovik, A. S. *J. Am. Chem. Soc.* **2006**, *128*, 15476−15489.
(32) Sahu, S.; Widger, L. R.; Quesne, M. G.; de Visser, S. P.; Matsumura, H.; Moënne- Loccoz, P.; Siegler, M. A.; Goldberg, D. P. *J. Am. Chem. Soc.* **2013**, *135*, 10590−10593.
(33) Widger, L. R.; Davies, C. G.; Yang, T.; Siegler, M. A.; Troeppner, O.; Jameson, G. N. L.; Ivanović-Burmazović, I.; Goldberg, D. P. *J. Am. Chem. Soc.* **2014**, *136*, 2699−2702.
(34) Widger, L. R.; Jiang, Y.; McQuilken, A. C.; Yang, T.; Siegler, M. A.; Matsumura, H.; Moënne-Loccoz, P.; Kumar, D.; de Visser, S. P.; Goldberg, D. P. *Dalton Trans.* **2014**, *43*, 7522−7532.
(35) Borovik, A. S. *Acc. Chem. Res.* **2005**, *38*, 54−61.
(36) Chatterjee, S.; Sheet, D.; Paine, T. K. *Chem. Commun.* **2013**, *49*, 10251−10253.
(37) Brivio, M.; Schlosrich, J.; Ahmad, M.; Tolond, C.; Bugg, T. D. H. *Org. Biomol. Chem.* **2009**, *7*, 1368−1373.
(38) Colabroy, K. L.; Zhai, H.; Li, T.; Ge, Y.; Zhang, Y.; Liu, A.; Ealick, S. E.; McLafferty, F. W.; Begley, T. P. *Biochemistry* **2005**, *44*, 7623−7631.
(39) APEX 2 *v2.1−0*, Bruker AXS, Madison, WI, 2006.
(40) Sheldrick, G. M. *SHELX97 Programs for Crystal Structure Analysis (Release 97−2)*; University of Göttingen: Göttingen, Germany, 1998.
(41) Frisch, M. J.; Trucks, G. W.; Schlegel, H. B.; Scuseria, G. E.; Robb, M. A.; Cheeseman, J. R.; Scalmani, G.; Barone, V.; Mennucci, B.; Petersson, G. A.; Nakatsuji, H.; Caricato, M.; Li, X.; Hratchian, H. P.; Izmaylov, A. F.; Bloino, J.; Zheng, G.; Sonnenberg, J. L.; Hada, M.; Ehara, M.; Toyota, K.; Fukuda, R.; Hasegawa, J.; Ishida, M.; Nakajima, T.; Honda, Y.; Kitao, O.; Nakai, H.; Vreven, T.; Montgomery, J. A., Jr.; Peralta, J. E.; Ogliaro, F.; Bearpark, M.; Heyd, J. J.; Brothers, E.; Kudin, K. N.; Staroverov, V. N.; Kobayashi, R.; Normand, J.; Raghavachari, K.; Rendell, A.; Burant, J. C.; Iyengar, S. S.; Tomasi, J.; Cossi, M.; Rega, N.; Millam, J. M.; Klene, M.; Knox, J. E.; Cross, J. B.; Bakken, V.; Adamo, C.; Jaramillo, J.; Gomperts, R.; Stratmann, R. E.; Yazyev, O.; Austin, A. J.; Cammi, R.; Pomelli, C.; Ochterski, J. W.; Martin, R. L.; Morokuma, K.; Zakrzewski, V. G.; Voth, G. A.; Salvador, P.; Dannenberg, J. J.; Dapprich, S.; Daniels, A. D.; Farkas, O.; Foresman, J. B.; Ortiz, J. V.; Cioslowski, J.;, and Fox, D. J. *Gaussian 09*, revision A.1; Gaussian, Inc.: Wallingford, CT, 2009.
(42) Lee, C.; Yang, W.; Parr, R. G. *Phys. Rev. B* **1988**, *37*, 785−789.
(43) Becke, A. D. *J. Chem. Phys. B* **1993**, *98*, 5648−5652.
(44) Petersson, G. A.; Al-Laham, M. A. *J. Chem. Phys.* **1991**, *94*, 6081−6090.
(45) McLean, A. D.; Chandler, G. S. *J. Chem. Phys.* **1980**, *72*, 5639−5648.
(46) Dunning, T. H., Jr.; Hay, P. J. In *Modern Theoretical Chemistry*; Schaefer, H. F.,III, Ed., Plenum: New York, 1976.

DOI: 10.1021/ic502658p
Inorg. Chem. XXXX, XXX, XXX−XXX